Applied and Computational Mathematics
2024; 13(5): 153-164
http://www.sciencepublishinggroup.com/j/acm
doi: 10.11648/j.acm.20241305.14
ISSN: 2328-5605 (Print); ISSN: 2328-5613 (Online)

Powell-Eyring Nanofluid Flow over a Stretching Sheet

Nictor Mwamba

Department of Applied Sciences and Engineering, Eden University, Lusaka, Zambia

Email address:
nictormk@gmail.com

To cite this article:
Nictor Mwamba. (2024). Powell-Eyring Nanofluid Flow over a Stretching Sheet. *Applied and Computational Mathematics, 13*(5), 153-164. https://doi.org/10.11648/j.acm.20241305.14

Received: 6 July 2024; **Accepted:** 26 August 2024; **Published:** 6 September 2024

Abstract: This research investigates the flow of a Powell-Eyring Nanofluid flowing over an exponentially stretching sheet. Thermal radiation, Soret, dissipation, and Dufour effects have been put into consideration. The obtained partial differential equations(PDE) have been transformed into ordinary differential equations (ODE) using similarity transformation. Numerical solutions are obtained in MATLAB using bvp4c frame work of fourth order accuracy integration scheme. It has been observed that the boundary layer for momentum increases with the velocity ratio while the boundary layers for thermal and concentration decrease. The velocity diminishes with increasing magnetic parameter while the temperature and concentration increased. The temperature increases with an increase in thermophoresis and Brownian motion. Increasing the fluid parameter resulted in decreased Nusselt number, skin friction, and Sherwood number. Increasing Powell-Eyring fluid parameter decreases the Nusselt number and Sherwood number but increases skin friction. This research may find use in the development of microelectronics, chemical processes, human targeted drug delivery, and heating and cooling system.

Keywords: Exponentially Stretching Sheet, Powell-Eyring Nanofluid, Chemical Reactions, Zero Mass Flux Condition

1. Introduction

The wide range of industrial applications of non-Newtonian fluids has lead to many recent studies[1-4]. Some of the fluids that exhibit non-Newtonian behavior include; lubricants, polymer solutions, drilling mud, various oils, paints, and ketchup.

Non-Newtonian fluids flowing over stretching surfaces is of great importance in electrochemistry and polymer industries. Generally, stretching surfaces are of different types, i.e., exponential stretching, linear and nonlinear stretching, radial stretching, and bidirectional stretching. Various researchers have studied non-Newtonian fluids' behavior in boundary layer domain [5-7]. Ferdows et al. [8] investigated the potential for thermal cooling in a convective non-Newtonian nanofluid that is flowing across a moving, expanding surface with a versatile power index. It was discovered that as free stream velocity values increased, boundary layers for temperature, velocity, and missing velocity and temperature slopes also increased, but that after a point of separation, the missing velocity and temperature slopes decreased. Kafunda et al. [9] explored the non-Newtonian nanofluid's unsteady hydromagnetic flow across a stretching sheet in the midst of a changing magnetic field and a chemical reaction. The applied magnetic field's angle of inclination was shown to have a negative effect on the velocity profile, but the temperature profile had the opposite effect. Patil et al. [10] studied the unsteady MHD flow of a Nano Powell-Eyring fluid at its stagnation point past a convectively heated stretched sheet in the presence of a chemical process involving thermal radiation. The results showed that the velocity of the fluid increased as the fluid parameter values increased, while the temperature and concentration decreased. Pal and Mondal [11] examined the combined effects of suction/injection-accounting magnetic field and chemical reaction, as well as the effects of nonlinear thermal radiation and Joule heating, on Powell Eyring nanofluid flow carrying gyrotactic microorganisms moving through a convectively heated stretching sheet. According to the results, adding nanoparticles to Powell-Eyring nanofluid lowers the concentration of nanoparticles by causing a chemical reaction and a fall in Schmidt number. The density of motile bacteria decreased as a result of the bioconvection Schmidt number and bioconvection Peclet number.

A Powell-Eyring fluid is a non-Newtonian fluid named

after Powell and Eyring and it was presented by them in 1944. The model of Powell-Eyring for fluids may be difficult to understand mathematically, but it offers distinct benefits compared to other non-Newtonian fluid models. Specifically, it is derived from the kinetic theory of liquids rather than relying on empirical relationships. Additionally, it accurately represents Newtonian behavior at both low and high shear rates. Most of the significant properties of Powell-Eyring fluids are discussed by [12-15]. Salah [16] studied a model for Powell-Eyring fluid with generalized heat flux and chemical reaction while considering radiation effects. A fluid velocity increase was discovered as the Powell-Eyring parameter increased while reverse behaviour was noticed for the temperature profile. It was also discovered that the fluid's temperature increases in response to an increase in the radiation parameter. Neseem et al. [17] Peter investigated the movement of heat through an exponentially extending sheet in an electrically conductive Eyring-Powell fluid. The study showed that the time it takes for thermal relaxation is negatively correlated with the thickness of the thermal boundary layer, but the Eckert number shows the opposite correlation.

Mushtaq et al. [18] proposed a mathematical model for the stagnation-point flow and heat transfer caused by an exponentially stretched sheet in a Powell-Eyring fluid. The shooting method and a fourth-order Runge-Kutta integration technique were used to obtain the numerical solutions. Among other results, it was observed that the velocity ratio affects the momentum boundary layer in a dual manner, while increasing the velocity ratio causes the thermal boundary layer to become thinner. A research on the Ree-Eyring nanofluid flow over a Riga plate using thermal radiation and bioconvention was conducted by Loganathan et al. [19]. The findings showed that when the radiation parameter and Biot number are increased, the fluid temperature rises, whereas higher Brownian moments and thermophoretic parameters have the opposite effect. It was also found that fluid velocity increases when the Weissenberg number is increased, and it decreases when the mixed convection parameter is increased. Ishaq et al. [20] explored the entropy production on nanofluid thin film flow of Eyring-Powell fluid with thermal radiation and the MHD effect on an unsteady porous stretching surface. The model was solved using the Homotopy analysis approach. It was found that entropy decreases with the increasing values of Eyring-Powell and radiation parameters. And also that the velocity distributions decreases with increasing magnetic parameter but the opposite effect was observed for entropy. Further, it was reported that porosity parameter decreases the motion of the liquid films. S. Reddy et al. [21] investigated the hydrodynamic movement of Eyring-Powell nanofluid within a stagnation point across an inclined cylinder under the influence of thermal radiation, Arrhenius activation energy, and binary chemical reaction. From some of the observations, it was noticed that the velocity of the fluid increases with large values of velocity ratio and that the concentration increases with an increase in temperature ratio parameter and activation energy. A numerical study was conducted by Khadar and Babatin [22] utilizing a Powell-Eyring fluid flow model over a layered stretched sheet with a magnetic field to enhance the cooling process. The findings demonstrated that although raising the heat generation or thermal conductivity parameter increases the temperature distribution, increasing the viscosity or slip velocity parameter decreases the velocity distribution. A numerical investigation of time-dependent magnetohydrodynamics (MHD) Eyring-Powell liquid by taking a moving/static wedge with Darcy Forchheimer relation was carried out by Ahmed et al. [23]. Thermal radiation was taken into consideration in order to predict solar radiation, and the concept of bioconvection was also taken into account in order to control the chaotic movement of floating nanoparticles. In the case of a static and moving wedge, it was found that the Forchheimer number causes the velocity field to decrease. Higher values of the bio convective Lewis number and Peclet number also degrade the motile density profiles.

The study of nanofluids has progressed over the years because of the demand that comes from their industrial and medical applications such as in heating and cooling systems, chemical processes, targeted drug transportation in human bodies, and in microelectronics. A combinations of a base fluid and suspended nanoparticles which are typically less than 100nm in size is known as a nanofluid. These nanoparticles can be made from various materials like metals, carbon based materials, and metal-oxides. Nanofluids presents the heat transfer enhancement performance and several studies have been conducted on nanofluids. Ali et al. [24] performed an irreversibility analysis on a hybrid nanofluid that comprised of carboxymethyl cellulose and water that was passing through a stretchable vertical sheet. The findings displayed that while temperature distribution and Bejan number increased, the velocity and entropy profiles decreased as the Weissenberg number increased. It was discovered that by increasing the value of the mixed Biot number and convective parameter, the drag friction and heat transfer rate were improved. The effects of couple stress and combined thermal radiations on heat energy transfer during 3D nanofluid (water-based) motion over a rotating surface was investigated by Ullah et al. [25]. It was discovered that the velocity increases with higher thickness and stress parameter values, while it decreases with higher nanoparticle volume fraction and rotation parameter values.

Khan et al. [26] looked at a radiative mixed convective flow caused by the nanofluid over a porous vertical cylinder with a mediam that was porous and an irregular heat source or sink. Y. D. Reddy et al. [27] looked into the numerical solution of a steady two dimensional magneto-hydrodynamic stagnation point flow of an incompressible nanofluid along a stretching cylinder. Additionally, the effects of radiation and convective boundary conditions were investigated, as well as thermophoresis and brownian motion. The findings showed that as the Biot number and radiation parameter values increased, there was a corresponding rise in nanoparticle volume fraction and temperature profile. Conversely, when the values of the brownian motion parameter and thermophoresis parameter increased, the heat transfer rate decreased. The

characteristics of thermal energy transfer during the migration of a hybrid nanofluid in the company of a fluctuating magnetic field, radiation, and a heat source was examined by Rizk et al. [28]. The outcome analysis showed that the Nusselt number and skin friction increase as the magnetic field's strength and concentration of nanomaterials increase. It was found that increased magnetic field strength leads to higher Lorentz forces, which causes the fluid velocity to constrict. Increased rotation speed also causes the fluid velocity to decrease. Additionally, it was observed that the fluid's temperature increases as the concentration of nanomaterials increases. Shah et al. [29] conducted an analysis to determine how Al2O3 nanoparticles would move through a hot, permeable cubic object while being affected by magnetic forces. The results obtained demonstrated effective conduction for higher magnetic number values. It was discovered that when nano powder is added to the base fluid, thermal conductivity always increases.

From the discussed literature above, there has been no attempts made to study the Powell-Eyring nanofluid flow over a stretching sheet taking into consideration thermal radiation, dissipation effects, Soret and Dufour effects.

2. Mathematical Formulation

Figure 1 shows the boundary layers for heat and momentum of the Powell-Eyring nanofluid that is incompressible. The stress tensor for a Powell-Eyring model [30] is given by:

$$\tau_{ij} = \mu \frac{\partial u_i}{\partial x_j} + \frac{1}{\beta} sinh^{-1}\left(\frac{1}{C_1}\frac{\partial u_i}{\partial x_j}\right) \tag{1}$$

where C_1, and β are the Powell-Eyring fluid's material parameters such that

$$sinh^{-1}\left(\frac{1}{C_1}\frac{\partial u_i}{\partial x_j}\right) = \frac{1}{C_1}\frac{\partial u_i}{\partial x_j} - \frac{1}{6}\left(\frac{1}{C_1}\frac{\partial u_i}{\partial x_j}\right)^3, \left|\frac{1}{C_1}\frac{\partial u_i}{\partial x_j}\right| \ll 1 \tag{2}$$

The velocity of the stretching sheet is along the x-axis and is given by $U_w(x) = ae^{\frac{x}{l}}$. The fluid temperature at the plate's surface of is given by $T_w(x) = T_\infty + ce^{\frac{x}{2l}}$ and the concentration is $C_w(x) = C_\infty + de^{\frac{x}{2l}}$. The ambient velocity, temperature, and concentration is denoted by U_∞, T_∞, and C_∞ respectively [16, 17].

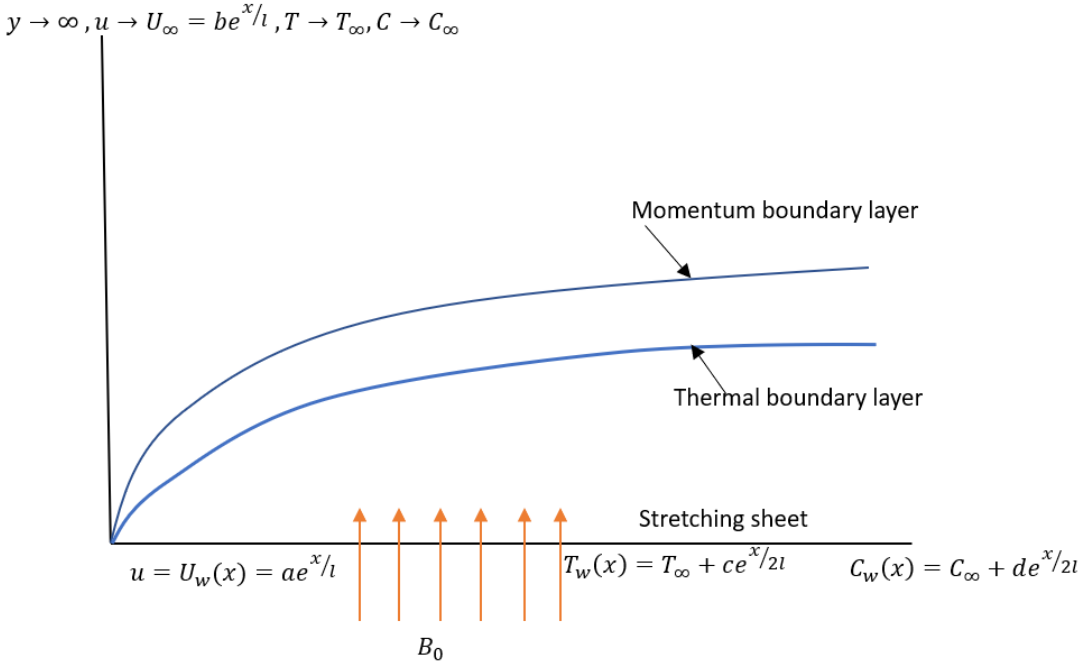

Figure 1. *Geometrical configuration of the flow over an exponentially stretching sheet.*

The equations governing this flow problem are as follows [16, 17, 31]:

$$\frac{\partial u}{\partial x} + \frac{\partial v}{\partial y} = 0 \tag{3}$$

$$u\frac{\partial u}{\partial x}+v\frac{\partial u}{\partial y}=\beta_t g(T-T_\infty)+\beta_c g(C-C_\infty)+\left(\nu_{nf}+\frac{1}{\rho_{nf}\beta C_1}\right)\frac{\partial^2 u}{\partial y^2} \tag{4}$$
$$-\frac{1}{2\rho_{nf}\beta C_1^3}\left(\frac{\partial u}{\partial y}\right)^2\frac{\partial^2 u}{\partial y^2}-\frac{\sigma_{nf}B_0^2(u_\infty-u)}{\rho_{nf}}$$

$$u\frac{\partial T}{\partial x}+v\frac{\partial T}{\partial y}=\frac{k_{nf}}{(\rho C_p)_{nf}}\left(\frac{\partial T}{\partial y}\right)^2+\frac{(\rho C_p)_s}{(\rho C_p)_f}\left[D_B\frac{\partial C}{\partial y}\frac{\partial T}{\partial y}+D_T\left(\frac{\partial T}{\partial y}\right)^2\right] \tag{5}$$
$$+\frac{\sigma_{nf}B_0^2u^2}{(\rho C_p)_{nf}}-\frac{1}{(\rho C_p)_{nf}}\frac{\partial q}{\partial y}+\frac{1}{(\rho C_p)_{nf}}\left(\mu_{nf}+\frac{1}{\beta C_1}\right)\left(\frac{\partial u}{\partial y}\right)^2-\frac{1}{(\rho C_p)_{nf}}\frac{1}{6\beta C_1^3}\left(\frac{\partial u}{\partial y}\right)^4$$

$$u\frac{\partial C}{\partial x}+v\frac{\partial C}{\partial y}=D_B\frac{\partial^2 C}{\partial y^2}+\frac{D_TK_T}{T_\infty}\left(\frac{\partial^2 T}{\partial y^2}\right)-k_r(C-C_\infty) \tag{6}$$

Table 1. *Termo-physical characteristics formulas.*

Properties	Nanofluid
Dynamic viscosity	$\mu_{nf}=\mu_f(1-\phi)^{-2.5}$
Density	$\rho_{nf}=(1-\phi)\rho_f+\phi\rho_s$
Heat capacity	$(\rho C_p)_{nf}=(1-\phi)(\rho C_p)_f+\phi(\rho C_p)_s$
Thermal conductivity	$\frac{k_{nf}}{k_f}=\frac{k_s+(m-1)k_f-(m-1)\phi(k_f-k_s)}{k_s+(m-1)k_f+\phi(k_f-k_s)}$
Electric conductivity	$\frac{\rho_{nf}}{\rho_f}=\left[1+\frac{3\left(\frac{\sigma_s}{\sigma_f}-1\right)\phi}{\left(\frac{\sigma_s}{\sigma_f}2+\right)-\left(\frac{\sigma_s}{\sigma_f}-1\right)}\right]$

where β_c, β_t, and g are the concentration expansion and volumetric thermal coefficients, and gravitational constant respectively. The temperatures of the fluid and the wall are denoted by T and T_w, respectively. C, C_w, ν_{nf}, C_{pf}, C_{ps}, ρ_f, ρ_s, and ρ_{nf} represent, respectively, the concentration, concentration at the wall, kinematic viscosity of the nanofluid, specific heat capacity of the base fluid, specific heat capacity of the nanoparticles, density of the base fluid, density of the nanoparticles, and density of the nanofluid. B_0, σ_{nf}, D_B, D_T, q, K_T, and k_r denote the magnetic field, electrical conductivity of the nanofluid, Brownian diffusion coefficient, thermophoresis diffusion coefficient, radiation heat flux, thermal diffusion ratio, and chemical reaction coefficient, respectively.

By the Rosselands approximation for radiation, $q=\frac{4\sigma*}{3\kappa^*}\frac{\partial T^2}{\partial y}$ where κ^* is the absorption coefficient and σ^* is the Stefan Boltzmann constant. Expanding T^2 in Tylor series about T_∞ and neglecting higher orders, the relation $T^2=4T_\infty^3T-3T_\infty^4$ is obtained.

The following are the relevant boundary conditions:

$$u=U_w(x)=ae^{\frac{x}{l}},\ v=0, T=T(w)=T_\infty+ce^{\frac{x}{2l}},$$
$$C_w(x)=C_\infty+de^{\frac{x}{2l}},\ at\ y=0$$
$$u\longrightarrow U_\infty(x)=be^{\frac{x}{l}},\ T\longrightarrow T_\infty,\quad C\longrightarrow C_\infty\ at\ y\longrightarrow\infty \tag{7}$$

To convert the aforementioned partial differential equations (PDE) into ordinary differential equations (ODE), the similarity transformation variables listed below are applied [16, 18]:

$$\eta=\sqrt{\frac{a}{2\nu_{nf}l}}e^{\frac{x}{2l}}y, u=ae^{\frac{x}{l}}f'(\eta)$$
$$v=-\sqrt{\frac{a\nu_{nf}}{2l}}e^{\frac{x}{2l}}[f(\eta)+\eta f^{'}(\eta)], \tag{8}$$
$$\theta(\eta)=\frac{T-T_\infty}{T_w-T_\infty},\ \phi(\eta)=\frac{C-C_\infty}{C_w-C_\infty} \tag{9}$$

Applying the above similarity transformation to the system of PDEs (5)-(6) the following ODEs are obtained.

$$(1+K)f'''+ff''-K\Gamma f''^2f'''+\frac{2}{Re^2}(cG_r\theta+dG_c\phi)-M(\lambda-f')=0 \tag{10}$$

$$\frac{1}{Pr}(Rd+1)\theta'' + N_b\phi'\theta' + N_t\theta'^2 + \theta' f + MEcf'^2 + Ec(1+K)f''^2 - \frac{1}{3}Ec\Gamma K f''^4 = 0 \tag{11}$$

$$\phi''\left(f + \frac{1}{Sc}\right) + Sr\theta'' - 2\Gamma_1\phi = 0 \tag{12}$$

$$\begin{array}{lllll} f(0)=0 & f'(0)=1 & \theta(0)=1 & \phi(0)=1 & at\ \ \eta=0 \\ f'(\infty)=\lambda & \theta(\infty)=0 & \phi(\infty)=0 & at\ \ \eta\longrightarrow\infty & \end{array} \tag{13}$$

such that

$$\begin{array}{lll} Re=\dfrac{lae^{\frac{x}{l}}}{\nu_{nf}} & \Gamma_1=\dfrac{k_r l}{U_w} & Pr=\dfrac{(\nu\rho C_p)_{nf}}{\kappa} \\ Ec=\dfrac{U_w^3}{C_{p_{nf}}ce^{\frac{x}{2l}}} & M=\dfrac{2l\sigma_{nf}B_0^2}{\rho_{nf}U_w} & Gr=\dfrac{g\beta ce^{\frac{x}{2l}}l^3}{\nu_{nf}^2} \end{array}$$

$$\begin{array}{lll} Sc=\dfrac{\nu_{nf}}{D_B} & Sr=\dfrac{DK_T ce^{\frac{x}{2l}}}{\nu_{nf}T_\infty de^{\frac{x}{2l}}} & K=\dfrac{1}{\mu_{nf}\beta C_1} \\ \Gamma=\dfrac{U_w^3}{4lC_1\nu_{nf}} & Rd=\dfrac{16\sigma^*T_\infty^3}{3\kappa^*\kappa} & Gr_c=\dfrac{g\beta de^{\frac{x}{2l}}l^3}{\nu_{nf}^2} \\ N_b=\dfrac{(\rho C_p)_s D_B de^{\frac{x}{2l}}}{(\rho C_p)_f\nu_{nf}} & N_t=\dfrac{(\rho C_p)_s D_T ce^{\frac{x}{2l}}}{(\rho C_p)_f T_\infty\nu_{nf}} & \lambda=\dfrac{b}{a} \end{array} \tag{14}$$

where the Reynolds number is Re, the chemical reaction parameter is Γ_1, the Eckert number is Ec, the Prandtl number is Pr, the magnetic number is M, the thermal Grashof number is Gr, the Schmidt number is Sc, the Soret number is Sr, the Powell-Erying fluid parameters are K and Γ, the radiation parameter is Rd, the concentration Grashof number is Gr_c, the Brownian motion parameter is N_b, the thermophoresis parameter is N_t, and the velocity ratio is λ.

The skin friction coefficient (C_f), Sherwood number (Sh), and Nusselt number (Nu) are among the other numbers of relevance [16,32].

$$C_f = \frac{\tau_w}{\rho U_w^2},\ \ Nu_x = \frac{xq_w}{kce^{\frac{x}{2l}}},\ \ Sh = -\frac{xq_m}{Dde^{\frac{x}{2l}}} \tag{15}$$

where τ_w denotes the surface skin shear stress, q_w represents the heat flux, and q_m signifies the mass flux, as defined by the following equation:

$$\begin{aligned} \tau_w &= \left[\left(\mu_{nf} + \frac{1}{\beta C_1}\right) - \frac{1}{6\beta C_1^3}\left(\frac{\partial u}{\partial y}\right)^3\right] \text{ at } y=0, \\ q_w &= -k\left(1 + \frac{16\sigma^* T_0^3}{3\kappa^* k_{nf}}\right)\frac{\partial T}{\partial y} \text{ at } y=0, \\ q_m &= -D\frac{\partial C}{\partial y} \text{ at } y=0 \end{aligned} \tag{16}$$

By applying the non-dimensional numbers (14) and the equations (7) and (16) to (15), the skin friction, Nusselt number, and Sherwood number can be expressed as follows:

$$\begin{aligned} \sqrt{2Re}C_f &= (1+K)f''(0) - \frac{K\Gamma}{3}(f''(0))^3, \\ Nu_x\left(\frac{xRe_x}{2l}\right)^{-\frac{1}{2}} &= -(1+Rd)\theta' \\ Sh_x\left(\frac{Re_x}{2}\right)^{-\frac{1}{2}}\left(\frac{l^2}{x}\right)^{\frac{1}{2}} &= -\phi'(0) \end{aligned} \tag{17}$$

3. Numerical Solution

Agrawal and Kaswan [32] employed a fourth-order precision methodology (bvp4c) and the homotopy analysis method to solve the Eyring-Powell fluid model. Other authors have used the bvp4c [17,33,34]. The numerical solutions are obtained using the bvp4c MATLAB solver, a finite difference code that utilizes the three-stage Lobatto IIIa formula. Equations (10), (11), and (12) are converted into difference equations as shown below. The flowchart illustrating the numerical scheme is presented in Figure 2.

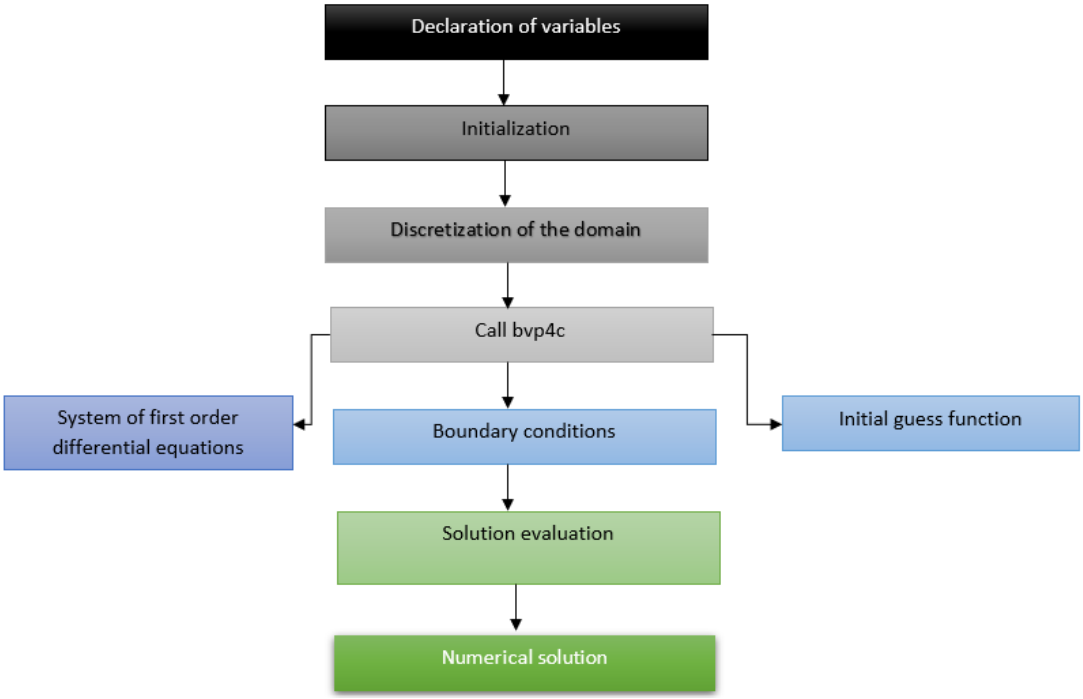

Figure 2. *Numerical scheme.*

$$f = y_1 \qquad f^{'} = y_2 \qquad f^{''} = y_3$$
$$\theta = y_4 \qquad \theta^{'} = y_5 \qquad \phi = y_6 \qquad \phi^{'} = y_7 \tag{18}$$

$$\begin{bmatrix} y_1^{'} \\ y_2^{'} \\ y_3^{'} \\ y_4^{'} \\ y_5^{'} \\ y_6^{'} \\ y_7^{'} \end{bmatrix} = \begin{bmatrix} y_2 \\ y_3 \\ \frac{M(\lambda - f') - \frac{2}{Re^2}(cG_r\theta + dG_c\phi) - ff''}{(1+K) - K\Gamma f''^2} \\ y_5 \\ \frac{\frac{1}{3}Ec\Gamma K f''^4 - (N_b\phi'\theta' + N_t\theta'^2 + \theta' f + MEcf'^2 + Ec(1+K)f''^2)}{\frac{1}{Pr}(Rd+1)} \\ y_7 \\ \frac{2\Gamma_1\phi - Sr\theta''}{\left(f + \frac{1}{Sc}\right)} \end{bmatrix} \tag{19}$$

The boundary conditions are as follows.

$$y_1 = 0 \qquad y_2 = 1 \qquad y_4 = 1 \qquad y_6 = 1$$
$$y_2 = \lambda \qquad y_4 = 0 \qquad y_6 = 0 \tag{20}$$

4. Results and Discussion

This section discusses the results and observations of the current research.

4.1. Velocity Profiles

An observation has been made in Figure 3, and it shows that the fluid velocity increases with a rise in Powell Eyring fluid parameter K. This can be attributed to the reduced viscosity as K increases, which leads to a higher velocity. The temperature gradient upsurge as the thermal Grashof number G_r increases as shown in Figure 4. This results in the buoyancy force leading to an increase fluid velocity. A similar trend is observed for the concentration Grashof number in Figure 5.

According to Figure 6, an increment in the magnetic number lowers the velocity profile. This is because an increase in the magnetic number implies that a flow resisting force, known as Lorentz force is enhanced. The velocity increases a λ increase as shown in Figure 7.

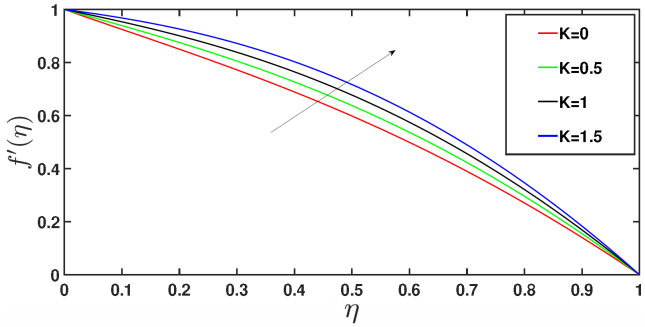

Figure 3. *Influence of K on $f'(\eta)$.*

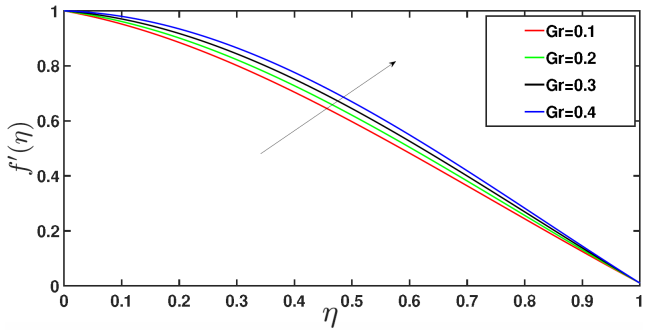

Figure 4. *Influence of G_r on $f'(\eta)$.*

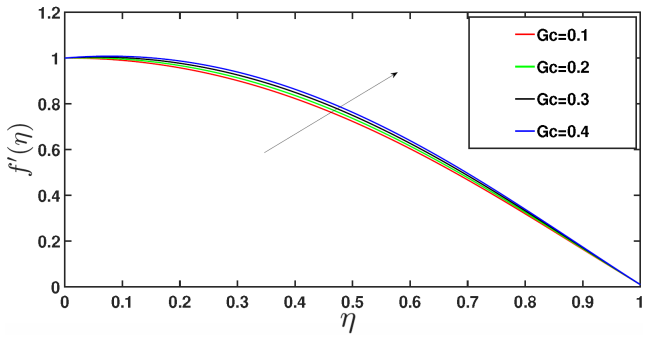

Figure 5. *Influence of G_c on $f'(\eta)$.*

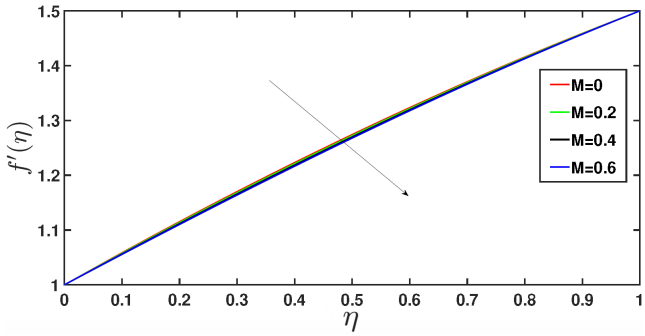

Figure 6. *Influence of M on $f'(\eta)$.*

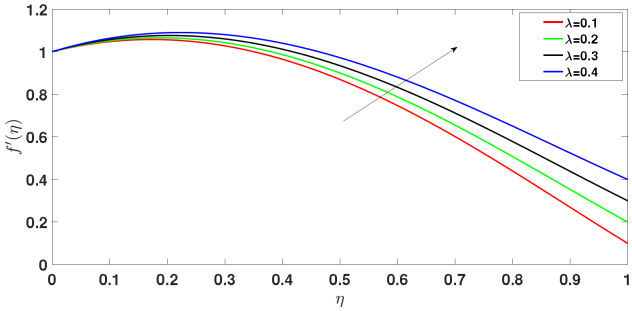

Figure 7. *Influence of λ on $f'(\eta)$.*

4.2. Temperature Profiles

Figure 8 illustrates the effects of Ec on the temperature profile. According to the findings, as Ec increases, the heat transfer rate at the plate's wall reduces, resulting in a thicker thermal boundary layer. This leads to an increase in fluid temperature.

The fluid temperature drops with heightening Powell-Eyring parameter. Enlargement of the values of Γ imply that the fluid is less viscous which reduces the fluid's thermal boundary layer and its dispassion effects. Therefore the temperature of the fluid drops as shown in Figure 9.

The thermal boundary layer diminishes as K values grow. This enhances the heat transfer rate of the flat plate which then lowers the temperature. Therefore, the profile for temperature drops as shown in Figure 10.

In Figure 11, the temperature profile grows with an enhancement in the magnetic parameter M. Joule heating is enhanced with an increase in the magnetic filed which results in an increased fluid temperature.

Figure 12 shows the temperature profile with different Brownian motion factor (Nb) values. Increasing the value of Nb leads to higher temperatures.

The temperature profile in Figure 13 demonstrates an inverse relationship with the thermophoresis parameter Nt. Growing values of the thermophoresis parameters Nt causes more random movement, which raises the temperature and reduces the nanoparticle volume fraction.

Figure 14 shows that the temperature upsurges with enhanced Pr. The thermal boundary layer is lowered as Pr rises. Therefore, heat is transmitted rapidly leading to a temperature drop.

The temperature profile in Figure 15 shows that the fluid's temperature exacerbates with higher values of Rd. This is associated to the heat flux from the plate that increases with an increase in Rd.

Figure 16 illustrates the influence of alterations in the velocity ratio parameter on the temperature profile. It has been noted that when λ grows, temperature falls.

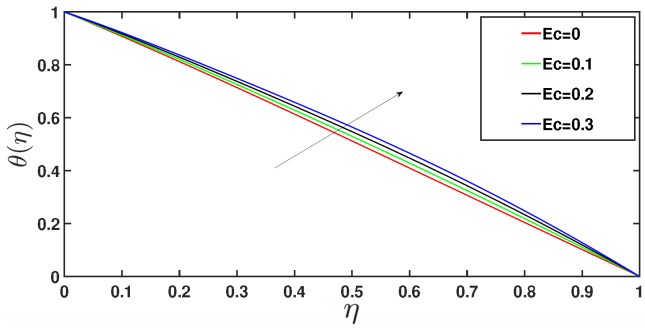

Figure 8. *Influence of E_c on $\theta(\eta)$.*

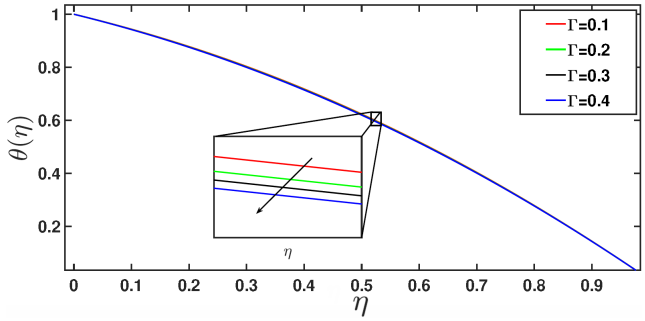

Figure 9. *Influence of Γ on $\theta(\eta)$.*

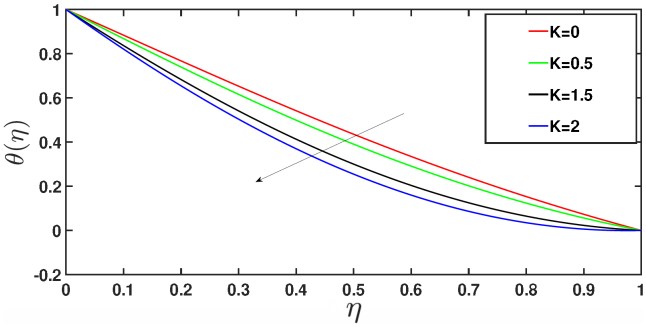

Figure 10. *Influence of K on $\theta(\eta)$.*

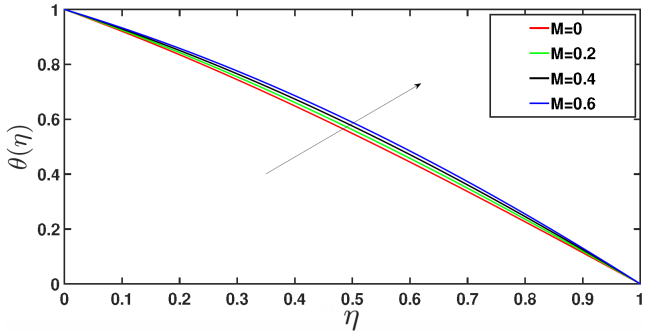

Figure 11. *Influence of M on $\theta(\eta)$.*

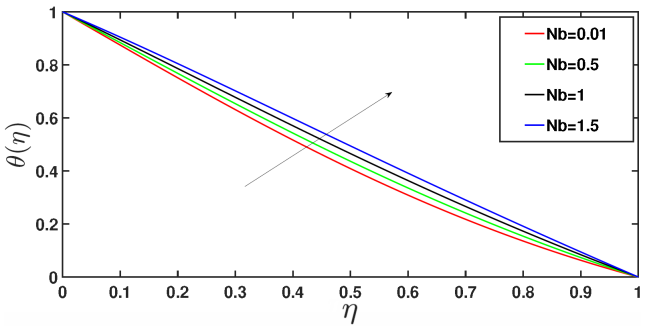

Figure 12. *Influence of Nb on $\theta(\eta)$.*

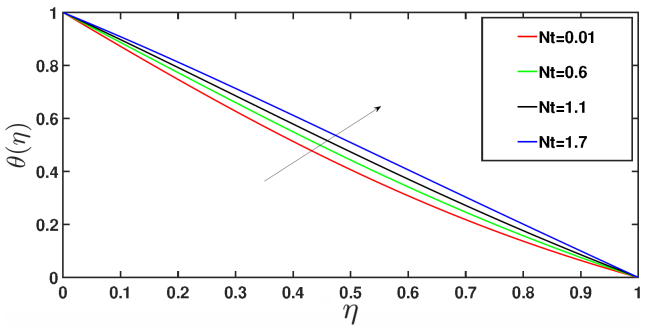

Figure 13. *Influence of Nt on $\theta(\eta)$.*

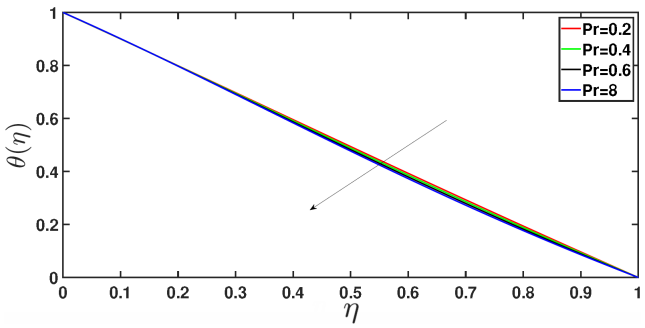

Figure 14. *Influence of Pr on $\theta(\eta)$.*

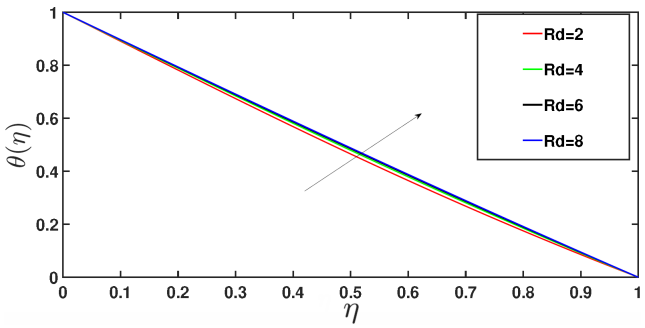

Figure 15. *Influence of Rd on $\theta(\eta)$.*

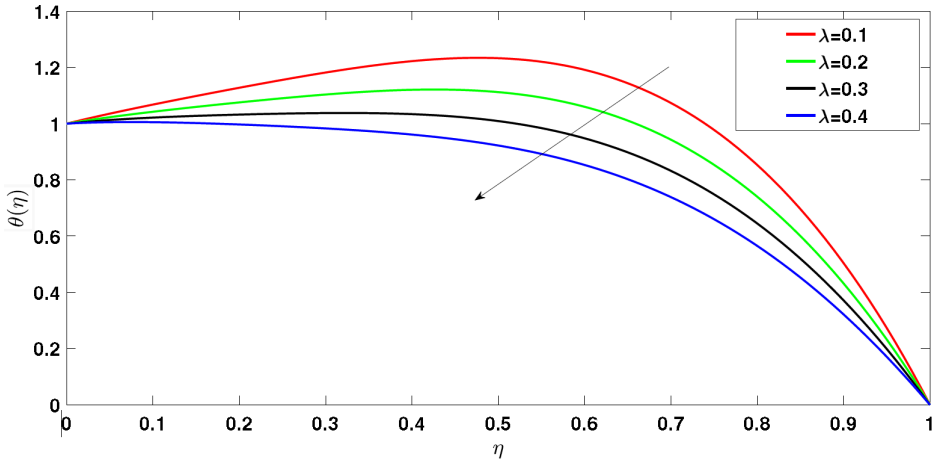

Figure 16. *Influence of* λ *on* $\theta(\eta)$.

4.3. Concentration Profiles

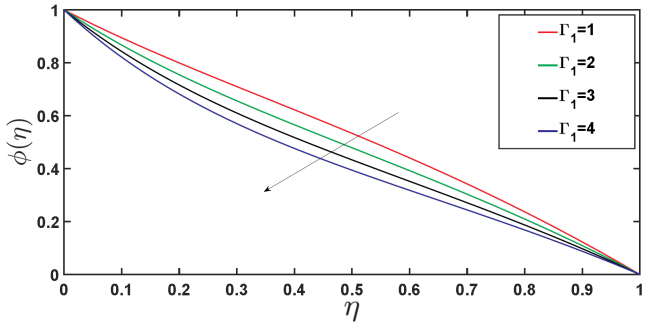

Figure 17. *Influence of* Γ_1 *on* $\phi(\eta)$.

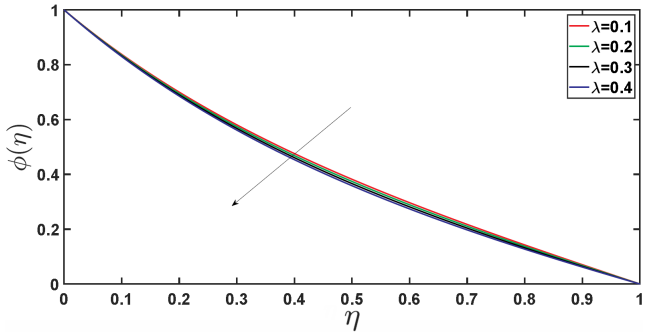

Figure 18. *Influence of* λ *on* $\phi(\eta)$.

Chemical molecular diffusivity diminishes when reaction parameters rise because the species are consumed in the process. Consequently, an inference can be made from Figure 17 that the concentration field diminishes as the values of the chemical reaction parameter augments. The concentration profile drops for increasing λ as depicted in Figure 17. An enhanced concentration boundary layer results from elevating values of λ. Figure 19 shows how the Schmidt number affects concentration. There is a fall in the concentration with increased S_c. From Figure 20, it has been noted that the fluid medium's concentration grows in tandem with an increase in the Soret number. Higher Soret numbers signify greater temperature gradients, leading to increased convective flow and consequently an enhanced concentration distribution. However, as one approaches the wall, where the temperature gradient decreases, the Soret effect weakens. Thus, a thinner concentration boundary layer is obtained by raising the Soret number.

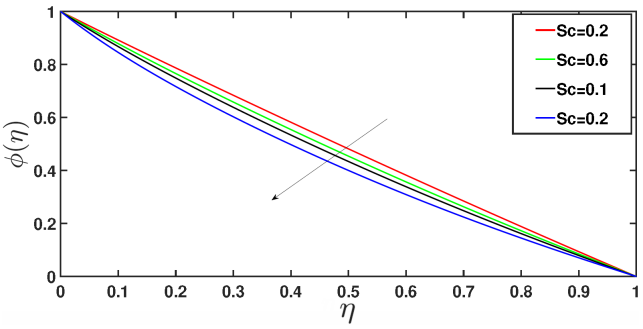

Figure 19. *Influence of* Sc *on* $\phi(\eta)$.

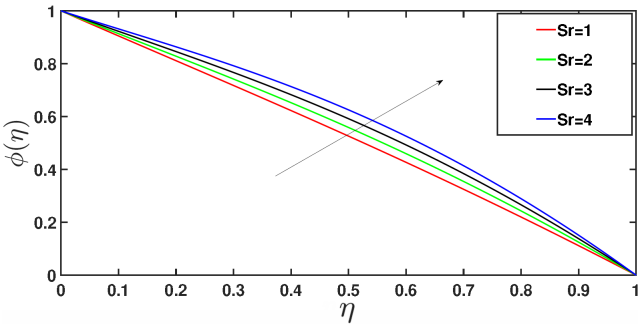

Figure 20. *Influence of* Sr *on* $\phi(\eta)$.

4.4. Effects of Variation of Parameters on Skin Friction, Nusselt and Sherwood Number

Table 2 presents the local Nusselt number, Skin-friction, and Sherwood number across various parameter values. As

K increases, the skin friction coefficient also increases. A comparable trend is seen in the Nusselt and Sherwood numbers as K increases. As the values of λ increase, the Nusselt and Sherwood numbers decrease, but the skin friction coefficient rises. When there is an increase in the Powell-Erying fluid parameter Γ, the skin friction coefficient, Nusselt number, and Sherwood number decrease. Raising the Prandtl number Pr results in higher Nusselt and Sherwood numbers, but reduces the skin friction coefficient. As the magnetic number M increases, the skin friction coefficient rises, whereas the Nusselt and Sherwood numbers decrease. Other authors have noticed similar trends [17, 18, 36].

Table 2. *Skin friction coefficient, Nusselt and Sherwood numbers for various values of parameters.*

K	λ	Γ	Pr	M	C_f	Nu_x	Sh_x
0					0.4998	0.7754	2.5848
0.5					0.7412	0.8894	2.9646
1					0.9827	1.0049	3.3495
1.5					1.2241	1.1215	3.7382
	0.01				0.5239	0.7867	2.6225
	0.2				0.5240	0.7404	2.4679
	1				0.5245	0.5404	1.8014
	1.2				0.5246	0.4890	1.6301
		0			0.5248	0.7865	2.6217
		0.5			0.5206	0.7854	2.6181
		1			0.5165	0.7843	2.6145
		1.5			0.5123	0.7832	2.6109
			1.5		0.5239	0.8999	2.9996
			2		0.5239	0.9648	3.2162
			2.5		0.5241	1.0254	3.4181
			3		0.5239	1.0835	3.6116
				0	0.5242	0.5356	1.7853
				0.2	0.5243	0.4250	1.4167
				0.4	0.5244	0.2999	0.9998
				0.6	0.5245	0.1574	0.5245

5. Concluding Remarks

This study is about Powell-Eyring nanofluid flow over a stretching sheet where thermal radiation, dissipation, Sort, and Dofour effects have been put into consideration. The influence of various non-dimensional parameters on temperature, velocity, and chemical reaction of the fluid has been studied. Below are the notable finding of the study.

1. As the velocity ratio λ and the Powell-Eyring fluid parameter K increase, the velocity also increases; however, it decreases with a rise in the magnetic parameter M.
2. The velocity rises with the enhancement of Brownian motion (Nb), thermophoresis (Nt), and magnetic parameters (M), yet declines as the Powell-Eyring fluid parameters (K and Γ) and the velocity ratio (λ) increase.
3. When the velocity ratio λ, chemical reaction parameter Γ_1, Schmidt number Sc, and Soret number Sr increase, the concentration decreases. Otherwise, it increases.
4. A decrease in the skin friction, Nusselt number and Sherwood number after increasing the fluid parameter Γ has been observed. Increasing K enhances skin friction bt lowers the Nusselt number and Sherwood number.

ORCID

0000-0002-7288-287X (Nictor Mwamba)

Data Availability

The data used to support the findings of this research are available within the article and are also available from the corresponding author upon request.

Acknowledgments

The author acknowledge Eden University for providing a conducive environment for conducting research.

Conflict of Interest

The authors declares that there are no conflicts of interest.

References

[1] C. Fetecau, J. Zierep, R. Bohning, and C. Fetecau, "On the energetic balance for the flow of an oldroyd-b fluid due to a flat plate subject to a time-dependent shear stress," Computers & Mathematics with Applications, vol. 60, no. 1, pp. 74-82, 2010. https://doi.org/10.1016/j.camwa.2010.04.031.

[2] T. Hayat, M. Mustafa, and I. Pop, "Heat and mass transfer for soret and dufoura's effect on mixed convection boundary layer flow over a stretching vertical surface in a porous medium filled with a viscoelastic fluid," Communications in Nonlinear Science and Numerical Simulation, vol. 15, no. 5, pp. 1183-1196, 2010. https://doi.org/10.1016/j.cnsns.2009.05.062

[3] C. Fetecau, W. Akhtar, M. Imran, and D. Vieru, "On the oscillating motion of an oldroyd-b fluid between two infinite circular cylinders," Computers & Mathematics with Applications, vol. 59, no. 8, pp. 2836-2845, 2010. https://doi.org/10.1016/j.camwa. 2010.02.002

[4] T. Hayat, M. Nawaz, M. Awais, and S. Obaidat, "Axisymmetric magnetohydrodynamic flow of jeffrey fluid over a rotating disk," International journal for numerical methods in fluids, vol. 70, no. 6, pp. 764-774, 2012. https://doi.org/10.1002/fld.2714

[5] T. Hayat, M. Awais, and S. Obaidat, "Similar solution for three-dimensional flow in an oldroyd-b fluid over a stretching surface," International Journal for Numerical Methods in Fluids, vol. 70, no. 7, pp. 851-859, 2012. https://doi.org/10.1002/fld.2716

[6] T. Hayat, M. Awais, M. Qasim, and A. A. Hendi, "Effects of mass transfer on the stagnation point flow of an upper-convected maxwell (ucm) fluid," International Journal of Heat and Mass Transfer, vol. 54, no. 15-16, pp. 3777-3782, 2011. https://doi.org/10.1016/j.ijheatmasstransfer.2011.03.003

[7] D. Mukonda, T. Kafunda, C. Kasumo, and J. Stanley, "Analysis on heat and mass transfer in boundary layer non-newtonian nanofluid flow past a vertically stretching porous plate with chemical reaction, variable magnetic field and variable thermal conductivity," Advances in Applied Mathematics and Mechanics, vol. 11, pp. 2347-2529, May 2024.

[8] M. Ferdows, M. Shamshuddin, S. Salawu, and S. Sun, "Thermal cooling performance of convective non- newtonian nanofluid flowing with variant power-index across moving extending surface," Scientific Reports, vol. 12, no. 1, pp. 1-20, 2022. https://doi.org/10.1038/s41598-022-12333-y

[9] T. Kafunda, M. Kinyanjui, and K. Giterere, "Unsteady hydromagnetic non-newtonian nanofluid flow past a porous stretching sheet in the presence of variable magnetic field and chemical reaction," Journal of Applied Mathematics and Physics, vol. 11, no. 9, pp. 2545-2567, 2023. https://doi.org/10.4236/jamp.2023.119165

[10] V. S. Patil, A. B. Patil, S. Ganesh, P. P. Humane, and N. S. Patil, "Unsteady mhd flow of a nano powell-eyring fluid near stagnation point past a convectively heated stretching sheet in the existence of chemical reaction with thermal radiation," Materials Today: Proceedings, vol. 44, pp. 3767-3776, 2021. https://doi.org/10.1016/j.matpr.2020.11.860

[11] D. Pal and S. K. Mondal, "Magneto-bioconvection of powell eyring nanofluid over a permeable vertical stretching sheet due to gyrotactic microorganisms in the presence of nonlinear thermal radiation and joule heating," International Journal of Ambient Energy, vol. 43, no. 1, pp. 924-935, 2022. https://doi.org/10.1080/01430750.2019.1679253

[12] T. Hayat and S. Nadeem, "Aspects of developed heat and mass flux models on 3d flow of eyring-powell fluid," Results in Physics, vol. 7, pp. 3910-3917, 2017. https://doi.org/10.1016/j.rinp.2017.09.048

[13] T. Hayat and S. Nadeem, "Flow of 3d eyring-powell fluid by utilizing cattaneo-christov heat flux model and chemical processes over an exponentially stretching surface," Results in Physics, vol. 8, pp. 397-403, 2018. https://doi.org/10.1016/j.rinp.2017.12.038

[14] S. Ijaz and S. Nadeem, "A balloon model examination with impulsion of cu-nanoparticles as drug agent through stenosed tapered elastic artery," Journal of Applied Fluid Mechanics, vol. 10, no. 6, pp. 1773-1783, 2017. https://doi.org/10.29252/jafm.73.245.27892

[15] S. Ijaz and S. Nadeem, "A biomedical solicitation examination of nanoparticles as drug agents to minimize the hemodynamics of a stenotic channel," The European Physical Journal Plus, vol. 132, pp. 1-13, 2017.

[16] F. Salah, "Chemical reaction and generalized heat flux model for powell-eyring model with radiation effects," International Journal of Mathematics and Mathematical Sciences, vol. 2022, 2022. https://doi.org/10.1155/2022/4076426

[17] T. Naseem, I. Bibi, A. Shahzad, and M. Munir, "Analysis of heat transport in a powell-eyring fluid with radiation and joule heating effects via a similarity transformation," Fluid Dynamics and Materials Processing, 2022. https://doi.org/10.32604/fdmp.2022.021136

[18] A. Mushtaq, M. Mustafa, T. Hayat, M. Rahi, and A. Alsaedi, "Exponentially stretching sheet in a powell-eyring fluid: Numerical and series solutions," Zeitschrift für Naturforschung A, vol. 68, no. 12, pp. 791-798, 2013. https://doi.org/10.5560/ZNA.2013-0063

[19] K. Loganathan, N. Alessa, R. Jain, F. Ali, and A. Zaib, "Dynamics of heat and mass transfer: Ree-eyring nanofluid flow over a riga plate with bioconvection and thermal radiation," Frontiers in Physics, p. 990, 2022. https://doi.org/10.3389/fphy.2022.974562

[20] M. Ishaq, G. Ali, Z. Shah, S. Islam, and S. Muhammad, "Entropy generation on nanofluid thin film flow of eyring-powell fluid with thermal radiation and mhd effect on an unsteady porous stretching sheet," Entropy, vol. 20, no. 6, p. 412, 2018. https://doi.org/10.3390/e20060412

[21] S. Reddy, P. Bala Anki Reddy, and A. Rashad, "Activation energy impact on chemically reacting eyring-powell nanofluid flow over a stretching cylinder," Arabian Journal for Science and Engineering, vol. 45, pp. 5227-5242, 2020. https://doi.org/10.1007/s13369-020-04379-9

[22] M. Khader and M. Babatin, "Numerical study for improvement the cooling process through a model of powell-eyring fluid flow over a stratified stretching sheet with magnetic field," Case Studies in Thermal Engineering, vol. 31, p. 101-786, 2022. https://doi.org/10.1016/j.csite.2022.101786

[23] M. F. Ahmed, A. Zaib, F. Ali, et al., "Numerical computation for gyrotactic microorganisms in mhd radiative eyring-powell nanomaterial flow by a static/moving wedge with darcy-forchheimer relation," Micromachines, vol. 13, no. 10, p. 1768, 2022.

[24] F. Ali, T. A. Kumar, K. Loganathan, et al., "Irreversibility analysis of cross fluid past a stretchable vertical sheet with mixture of carboxymethyl cellulose water based hybrid nanofluid," Alexandria Engineering Journal, 2022. https://doi.org/10.1016/j.aej.2022.08.037

[25] A. Ullah, M. M. Selim, T. Abdeljawad, M. Ayaz, N. Mlaiki, and A. Ghafoor, "A magnetite-water-based nanofluid three-dimensional thin film flow on an inclined rotating surface with non-linear thermal radiations and couple stress effects," Energies, vol. 14, no. 17, p. 5531, 2021. http://dx.doi.org/10.3390/en14175531.

[26] U. Khan, A. Zaib, A. Ishak, et al., "Radiative mixed convective flow induced by hybrid nanofluid over a porous vertical cylinder in a porous media with irregular heat sink/source," Case Studies in Thermal Engineering, vol. 30, p. 101-711, 2022. https://doi.org/10.1016/j.csite.2021.101711

[27] Y. D. Reddy, B. S. Goud, M. R. Khan, M. A. Elkotb, and A. M. Galal, "Transport properties of a hydromagnetic radiative stagnation point flow of a nanofluid across a stretching surface," Case Studies in Thermal Engineering, vol. 31, p. 101-839, 2022. https://doi.org/10.1016/j.csite.2022.101839

[28] D. Rizk, A. Ullah, S. Elattar, et al., "Impact of the kkl correlation model on the activation of thermal energy for the hybrid nanofluid (go+ zno+ water) flow through permeable vertically rotating surface," Energies, vol. 15, no. 8, p. 2872, 2022. https://doi.org/10.3390/en15082872

[29] Z. Shah, P. Kumam, A. Ullah, S. N. Khan, and M. M. Selim, "Mesoscopic simulation for magnetized nanofluid flow within a permeable 3d tank," IEEE Access, vol. 9, pp. 135234-135244, 2021. https://doi.org/10.1109/ACCESS.2021.3115599

[30] A. M. Rashad, M. A. Nafe, and D. A. Eisa, "Heat generation and thermal radiation impacts on flow of magnetic eyring-powell hybrid nanofluid in a porous medium," Arabian Journal for Science and Engineering, vol. 48, no. 1, pp. 939-952, 2023. http://dx.doi.org/10.1007/s13369-022-07210-9

[31] A. Alsaedi, T. Hayat, S. Qayyum, and R. Yaqoob, "Eyring-powell nanofluid flow with nonlinear mixed convection: Entropy generation minimization?" Computer Methods and Programs in Biomedicine, vol. 186, p. 105-183, 2020. https://doi.org/10.1016/j.cmpb.2019.105183

[32] R. Agrawal and P. Kaswan, "Mhd eyring-powell nanofluid past over an unsteady exponentially stretching surface with entropy generation and thermal radiation," Heat Transfer, vol. 50, no. 5, pp. 4669-4693, 2021. http://dx.doi.org/10.1002/htj.22095

[33] N. Mwamba, J. Okelo Abonyo, and K. O. Awuor, "Effects of thermal radiation and chemical reaction on hydromagnetic fluid flow in a cylindrical collapsible tube with an obstacle," International Journal of Mathematics and Mathematical Sciences, vol. 2023, no. 1, p. 9 991-376, 2023. https://doi.org/10.1155/2023/9991376

[34] V. Kaigalula, J. A. Okelo, S. Mutua, and O. M. Muvengei, "Magneto-hydrodynamic flow of an incompressible fluid in a collapsible elastic tube with mass and heat transfer," Journal of Applied Mathematics and Physics, 2023. https://doi.org/10.4236/jamp.2023.1111211 [Online]. Available: https://api.semanticscholar.org/ CorpusID: 265004159

[35] L. F. Shampine, J. Kierzenka, M. W. Reichelt, et al., "Solving boundary value problems for ordinary differential equations in matlab with bvp4c," Tutorial notes, vol. 2000, pp. 1-27, 2000.

[36] M. M. Bhatti, T. Abbas, M. M. Rashidi, M. E.-S. Ali, and Z. Yang, "Entropy generation on mhd eyring-powell nanofluid through a permeable stretching surface," Entropy, vol. 18, no. 6, p. 224, 2016. https://doi.org/10.3390/e18040117